Journal of Statistical Physics, Vol. 46, Nos. 1/2, 1987

Liapunov Exponents in High-Dimensional Symplectic Dynamics

Roberto Livi,[1] Antonio Politi,[2] Stefano Ruffo,[1] and Angelo Vulpiani[3]

Received August 15, 1986

The existence of a thermodynamic limit of the distribution of Liapunov exponents is numerically verified in a large class of symplectic models, ranging from Hamiltonian flows to maps and products of random matrices. In the highly chaotic regime this distribution is approximately model-independent. Near an integrable limit only a few exponents give a relevant contribution to the Kolmogorov–Sinai entropy.

KEY WORDS: Liapunov exponents; Kolmogorov entropy; symplectic transformations; random matrices; thermodynamic limit; coupled oscillators.

1. INTRODUCTION

Relevant results have been obtained in the comprehension of the chaotic properties of dynamical systems with few degrees of freedom.[1] On the contrary, little is known when a large number of degrees of freedom is considered. In these cases one looks for some generic properties that also hold in the thermodynamic limit. This is, of course, a necessary requisite for establishing the basis of any statistical approach. In some cases, the study of the statistical spatial properties of a system even simplifies as the number of degrees of freedom is increased. A typical example comes from hydrodynamic turbulence: around the onset of chaos a few degrees of freedom are involved, but the dynamics strongly depends on the "details" (e.g., boundary conditions) and a statistical description is inappropriate. In the limit of high Reynolds numbers, i.e., fully developed turbulence, many

[1] Dipartimento di Fisica dell'Universita', 50125 Firenze, Italy, and INFN Sezione di Firenze.
[2] Istituto Nazionale di Ottica, 50125 Firenze, Italy.
[3] Dipartimento di Fisica dell'Universita' di Roma I, 00185 Roma, and GNSM-CISM Roma.

0022-4715/87/0100-0147$05.00/0

degrees of freedom interact and some statistical properties are universal (e.g., velocity correlations in the inertial range).

Thermodynamic limit properties were already observed in some previous papers,[2] where global statistical features, energy equipartition, for instance, were shown to be asymptotically independent of the number of degrees of freedom.

In this paper we present a detailed numerical investigation of a large class of models characterized by a symplectic structure, showing the existence of the thermodynamic limit for the spectrum of the Liapunov characteristic exponents (LCE) λ_i, $i=1,\ldots, 2N$ (where N is the number of degrees of freedom). More precisely, we shall see that, in the limit of large N, the function

$$L(i/N)=\lambda_i/\lambda^* \tag{1.1}$$

where $\lambda^*=\lim_{N\to\infty}\lambda_1(N)$, remains fairly constant independent of N. Accordingly, a Kolmogorov–Sinai entropy density h_{KS} can be introduced and remains finite for $N\gg 1$. Indeed, using Pesin's formula,[3] one has

$$h_{KS}=\frac{1}{N}\sum_{i=1}^{2N}\lambda_i\Theta(\lambda_i)=\frac{\lambda^*}{N}\sum_{i=1}^{N}L\left(\frac{i}{N}\right)\simeq I\lambda^* \tag{1.2}$$

where $\Theta(X)$ is the Heaviside function, and $I=\int_0^1 L(x)\,dx<1$. From a numerical point of view, the main problem is obviously the computation of I. However, we shall see that in strongly chaotic cases $I\simeq 0.5$ and consequently the computation of h_{KS} reduces to that of λ^*. Moreover, the asymptotic shape of the LCE spectrum provides, in the weakly chaotic regime, an indication of the mechanism of the onset of chaos.

The systems we are going to consider are Hamiltonian flows modeling chains of anharmonic oscillators (Section 2), symplectic maps (Section 3), and products of random symplectic matrices (Section 4). In all these cases we shall consider nearest neighbor interactions. Section 5 is devoted to some discussions and conclusions.

2. HAMILTONIAN FLOWS

In this section we consider Hamiltonian models of chains of interacting particles. The typical Hamiltonian is of the form

$$\mathcal{H}=\sum_{i=1}^{N}\left[\frac{p_i^2}{2}+\frac{1}{2}(q_{i+1}-q_i)^2+V_i(\mathbf{q},\{\mu\})\right] \tag{2.1}$$

where q_i, p_i are the canonical variables and $\{\mu\}$ indicates a set of parameters. In a previous paper[4] we have analyzed the Fermi–Pasta–Ulam (FPU) β-model, whose potential is

$$V_i(\mathbf{q}, \{\mu\}) = \frac{1}{4}\beta(q_{i+1} - q_i)^4 \tag{2.2}$$

observing that a limiting distribution of exponents indeed exists and it is almost linear $[L(x) \simeq 1 - x]$ at large energy densities ($\beta > 10$). We are here interested in studying the model dependence of these results. With this aim we introduce the following potentials:

$$V_i(\mathbf{q}, \{\mu\}) = \frac{1}{6}\beta(q_{i+1} - q_i)^6 \tag{2.3}$$

$$V_i(\mathbf{q}, \{\mu\}) = \frac{z}{(q_{i+1} - q_i)^{12}} - \frac{w}{(q_{i+1} - q_i)^6} \tag{2.4}$$

$$V_i(\mathbf{q}, \{\mu\}) = \frac{1}{2}m^2 q_i^2 + \frac{1}{4}g q_i^4 \tag{2.5}$$

Potential (2.3) is the simplest bounded higher order generalization of the FPU model. Potential (2.4) is the Lennard-Jones 6–12 model describing a realistic interaction in a crystal. Potential (2.5) is the discretization of the nonlinear Klein–Gordon field theory.

Imposing periodic boundary conditions ($p_1 = p_{N+1}, q_1 = q_{N+1}$), we find that the first three models turn out to have two constants of motion, namely energy and momentum, while in the fourth one, translational invariance is broken and the momentum is no longer conserved. The equations of motion have been integrated by means of the Verlet leap-frog algorithm, which preserves the symplectic structure of the Hamiltonian flux. The time step Δt has been chosen in the range (0.01, 0.1) such that energy is conserved within 0.1% up to integration times of the order of 10^4. The simulations have been performed on a CRAY1-XMP computer with a fully vectorialized FORTRAN program. The numerical method used for evaluating the LCE spectrum is sketched in the Appendix. Since the symplectic structure of the transformations here considered yields an antisymmetric spectrum ($\lambda_i = -\lambda_{2N-i+1}$), we have limited our numerical analysis to the computation of the positive part only.

Our control parameter is the energy density ε. A comparison of the amplitude of the first nonlinear terms in models (2.3) and (2.4) with that in the FPU β-model makes possible a rough estimate of the equipartition threshold, thus allowing us to perform simulations in parameter regions

where there is, presumably, a single stochastic component, and the LCE are independent of the initial condition. The situation is more complicated in model (2.5), where two opposite integrable limits exist. Indeed, besides the standard case $\varepsilon \to 0$, also the limit $\varepsilon \to \infty$ reduces the model to a set of decoupled quartic oscillators. Hence, one can expect that even in an intermediate range of ε values, the motion is not fully chaotic and the LCE might depend on the initial condition.

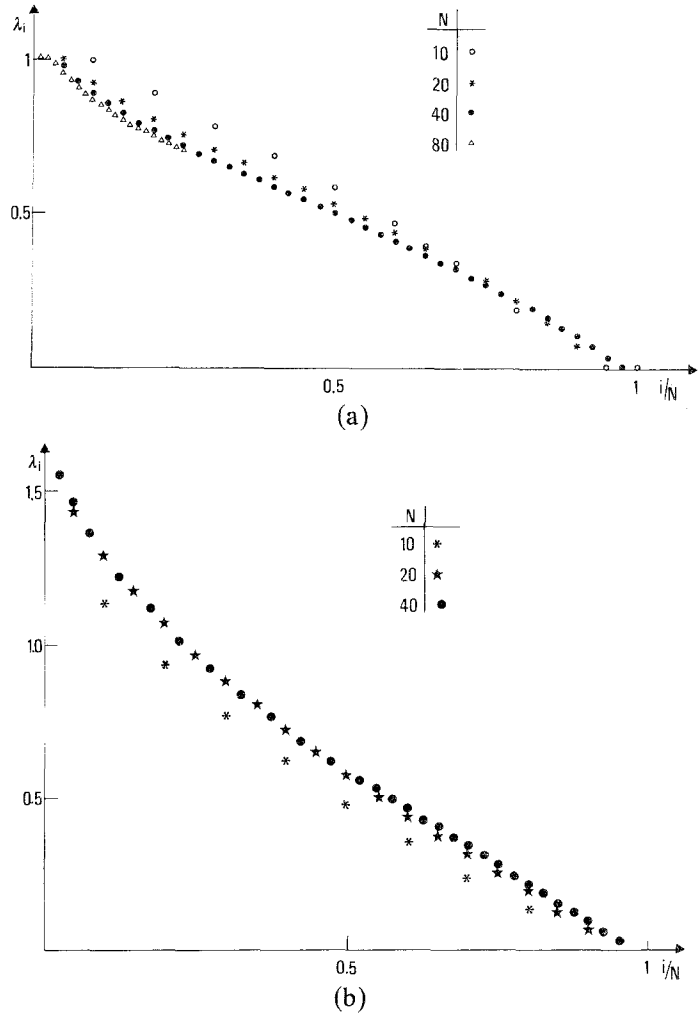

Fig. 1. Liapunov exponents λ_i versus i/N. (a) Model (2.3) with $\beta = 0.1$, $\varepsilon = 40$; (b) model (2.4) with $\varepsilon = 5.9$, $z = w = 1/36$; (c) model (2.5) with $m = 1$, $g = 1/3$, $\varepsilon = 47$; (d) model (2.4) with $\varepsilon = 60$, $z = w = 1/36$, $N = 20$.

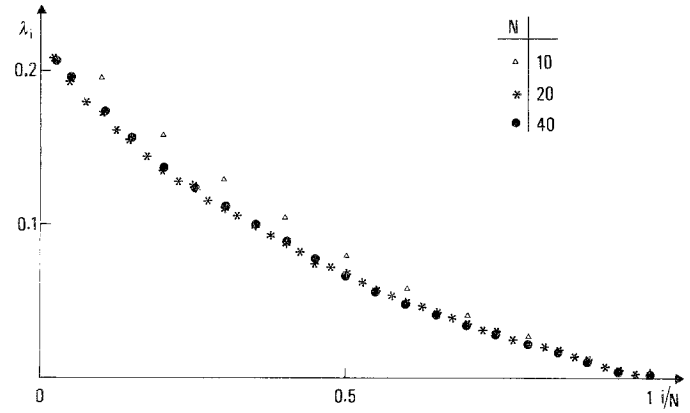

(c)

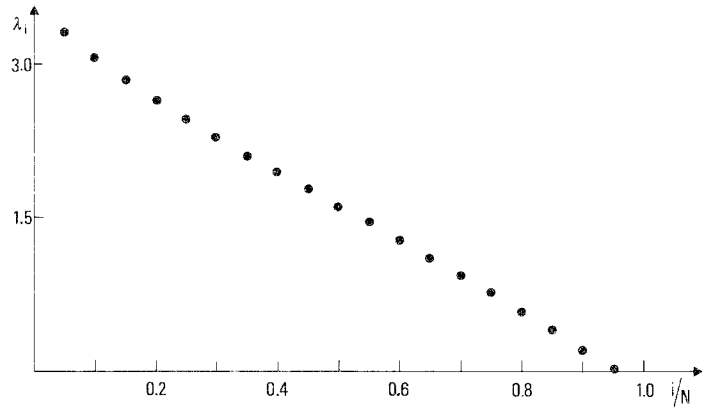

(d)

Fig. 1 (*continued*)

In Fig. 1 we show the resulting LCE spectrum for models (2.3)–(2.5). In all these cases a random initial condition has been chosen with $\sum_{i=1}^{N} p_i(t=0)=0$. Model (2.3) has been integrated for $\beta=0.1$, $\varepsilon=40$, and $N=10, 20, 40, 80$. In the last case only the 20 largest exponents have been computed. A nice convergence to a limit distribution is already obtained for $N=40$. The function $L(x)$ [see Eq. (1.1)] is almost a straight line even if deviations are definitely out of the numerical error, which is on the third significant figure in this case. Model (2.4) has been integrated with $z=w=1/36$, $\varepsilon=5.9$, and $N=10, 20, 40$, showing a good convergence already for $N=20$. The distribution becomes almost linear when the energy density is increased (see Fig. 1d).

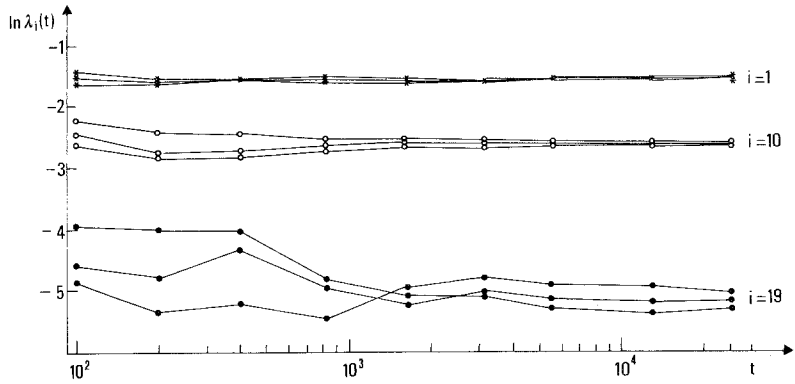

Fig. 2. Liapunov exponents λ_i versus t for model (2.5), $N=20$, $m=1$, $g=1/3$, $\varepsilon=50$, and with $i=1$, 10, 19. The results are reported for different, randomly chosen, initial conditions.

Finally, for model (2.5), we have chosen $m=1$, $g=1/3$, $\varepsilon=50$, and $N=20, 40$. At variance with the former cases, where an overall linear behavior of $L(x)$ has been found, here the distribution has a hyperbolic shape. This can be reasonably attributed to the previously mentioned absence of a strongly chaotic limit. For this reason, and in order to verify the independence of the initial condition, we have computed the LCE spectrum for three different choices of the initial conditions. The results for λ_1, λ_{10}, and λ_{19} are shown in Fig. 2 as a function of time, suggesting the existence of a single stochastic component in the phase space.

Comparing the results of these models, one can observe that the most relevant deviation from a linear distribution is in the region of low x values, where the curve shows an increasing slope. To investigate the dependence on ε of this phenomenon, we prefer to pass to symplectic maps, where one can push the numerical analysis to smaller ε values.

3. SYMPLECTIC MAPS

In the preceding section we showed the existence of a thermodynamic limit distribution for the LCE in Hamiltonian systems. Moreover, the spectrum turns out to be roughly linear, i.e., $L(x) \simeq (1-x)$, in highly chaotic regions.

In order to verify the generic properties of these results, we extend the analysis to symplectic maps of the form

$$\begin{aligned} \mathbf{q}(n+1) &= \mathbf{q}(n) + \mathbf{p}(n) \\ & \qquad \text{Mod}(2\pi) \qquad (3.1) \\ \mathbf{p}(n+1) &= \mathbf{p}(n) + \alpha \nabla F(\mathbf{q}(n+1)) \end{aligned}$$

where $\mathbf{q}$ and $\mathbf{p}$ are N-dimensional vectors depending on a discrete time n, and $\nabla = (\partial/q_1, ..., \partial/q_N)$. Let us point out that a symplectic map is a canonical transformation from the variables $(\mathbf{q}(n), \mathbf{p}(n))$ to $(\mathbf{q}(n+1), \mathbf{p}(n+1))$. Moreover, such map is interpretable as the recursive rule associated to a Poincaré section of a Hamiltonian system with $N+1$ degrees of freedom. In particular, for $\alpha = 0$, Eq. (3.1) represents a system of uncoupled harmonic oscillators ($\mathbf{p}$ being the actions and $\mathbf{q}$ the angles). When, instead, $\alpha \neq 0$, $F(\mathbf{q})$ plays a role analogous to the nonintegrable term in a Hamiltonian flux. Finally, let us notice that the LCE of Eq. (3.1), λ_i, are related to the LCE of the associated Hamiltonian flux Λ_i by the relation

$$\lambda_i = \tau \Lambda_i \tag{3.2}$$

where τ is the mean return time on the surface of section. In analogy with Section 2, we limit ourselves to nearest neighbor interactions and periodic boundary conditions, i.e.,

$$q_i(n+1) = q_i(n) + p_i(n) \quad \text{Mod}(2\pi) \tag{3.3a}$$

$$\begin{aligned} p_i(n+1) = p_i(n) + \alpha \{ & g[q_{i+1}(n+1) - q_i(n+1)] \\ & - g[q_i(n+1) - q_{i-1}(n+1)] \} \quad \text{Mod}(2\pi) \end{aligned} \tag{3.3b}$$

with $q_1 = q_{N+1}$ and $p_1 = p_{N+1}$. The procedure to compute the LCE for map (3.3) is analogous to that used in the Hamiltonian case (for technical details see the Appendix).

Since the q's are angular variables, it is natural to choose $g(x)$ as a periodic function. In particular, we have chosen $g(x) = \sin^n(x)$, $n = 1, 3, 5$. For $\alpha > 0.1$, an asymptotic form of the LCE spectrum is already attained for $N \simeq 10$, again showing a straight-line shape (see Fig. 3). We have verified that the introduction of random quenched couplings α_i with average value $\bar{\alpha}_i > 0.1$, which modifies Eq. (3.3b)

$$\begin{aligned} p_i(n+1) = p_i(n) & + \alpha_{i+1} g[q_{i+1}(n+1) - q_i(n+1)] \\ & - \alpha_i g[q_i(n+1) - q_{i-1}(n+1)] \quad \text{Mod}(2\pi) \end{aligned} \tag{3.4}$$

does not affect the previous results (see Fig. 4). This shows that the observed behavior does not depend on any hidden symmetry of (3.3).

For $\alpha < 0.1$ an asymptotic LCE spectrum is again obtained, but $L(x)$ is no longer a straight line. In particular, in this weakly chaotic regime, a behavior similar to that of Hamiltonian systems is observed: $L(x)$ is linear only in the region $x \simeq 1$, while for $x \simeq 0$ the function tends to depart from the linear behavior (see Fig. 5). This effect enhances as ε decreases. A quan-

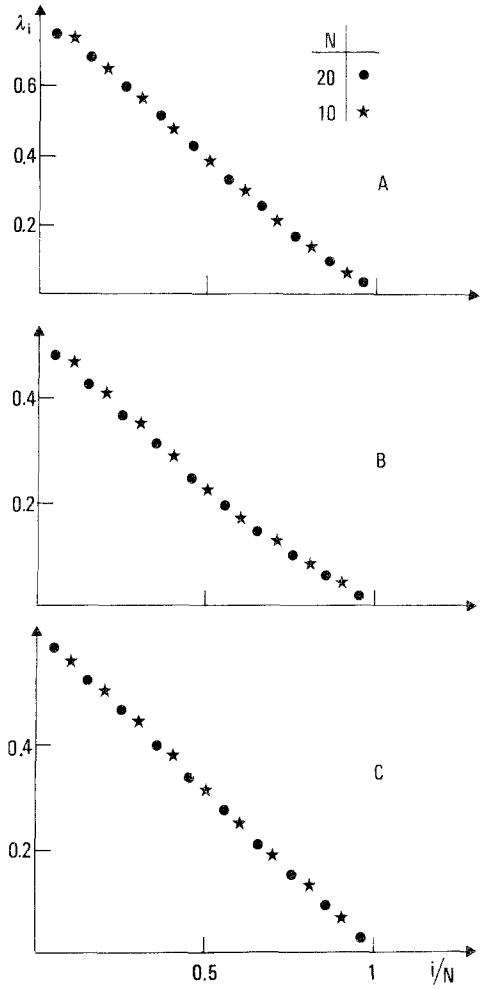

Fig. 3. Liapunov exponents λ_i versus i/N for the map (3.3). (A) $g(x)=\sin x$, $\alpha=1$; (B) $g(x)=\sin^3 x$, $\alpha=0.5$; (C) $g(x)=\sin^5 x$, $\alpha=0.6$.

titative analysis of this behavior has been performed by measuring the quantity

$$D=\frac{\lambda_1-\lambda_2}{\lambda_1}N \tag{3.5}$$

which is an estimate of the logarithmic derivative of $L(x)$ at $x=0$. While for $\alpha>0.05$, D is fairly constant around 1 (confirming the straight-line behavior of the spectrum), for α tending to zero, D increases reasonably

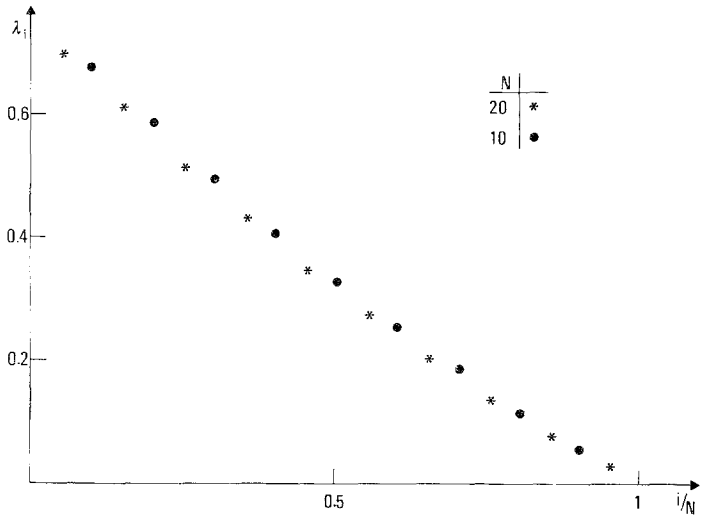

Fig. 4. Liapunov exponents λ_i versus i/N for the map (3.4), with $g(x) = \sin^3 x$, and α_i uniformly distributed in the interval [0.4, 1.2].

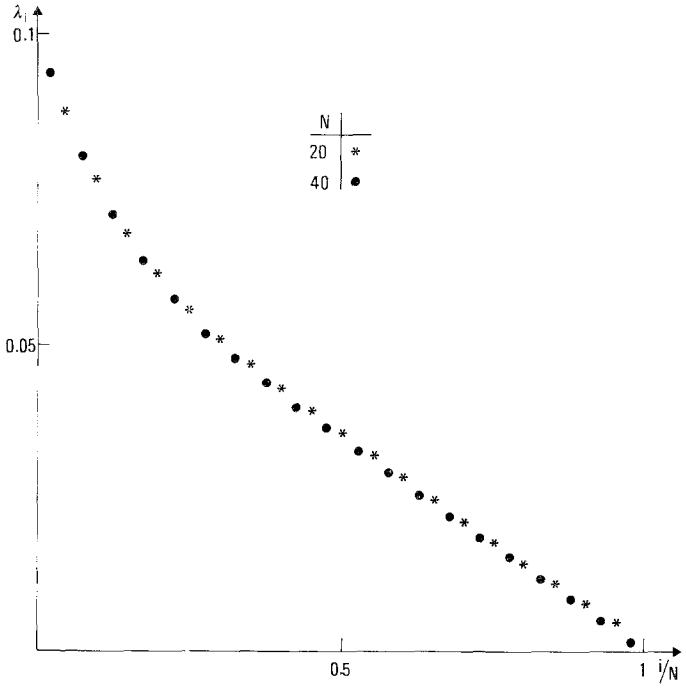

Fig. 5. Liapunov exponents λ_i versus i/N for the map (3.3), with $g(x) = \sin x$ and $\varepsilon = 0.02$.

fast (for $\alpha = 5 \times 10^{-3}$ we obtain an average value $D \simeq 8$ with $N = 40$). However, in this range of small α values, we start encountering the problem of an increasing dependence on the initial condition, which makes the estimate of the scaling behavior unfeasible. Referring, for instance, to $\alpha = 5 \times 10^{-3}$, we obtain (in different trials 10^8 iterations long) results oscillating between $D = 5$ and 11. The difference between these values is definitely out of the statistical errors, thus indicating that the phase space is (on that time scale) partitioned in disconnected stochastic components. However, the squeezing of the LCE spectrum against the y axis turns out to be, from our numerical simulations, unequivocal, as an increase of one order of magnitude in the derivative of Eq. (3.5) has been observed.

4. RANDOM MATRICES

The nearly straight line shape of the LCE spectrum, both in flows and maps, suggests the independence of this feature from the details of the dynamics. The simplest way to test this conjecture is by neglecting the deterministic correlations in the evolution of the tangent vectors.

The computation of the LCE involves, for the symplectic map (3.1), products of matrices of the form

$$A_\alpha(n) = \begin{bmatrix} 1 & 1 \\ \alpha a(n) & 1 + \alpha a(n) \end{bmatrix} \tag{4.1}$$

where 1 is the $N \times N$ identity matrix, and a_{ij} is the $N \times N$ symmetric matrix defined by

$$a_{ij}(n) = \partial^2 F / \partial q_i \, \partial q_j \tag{4.2}$$

where the derivative is evaluated in $\mathbf{q}(n)$. Here, we still multiply matrices of the form (4.1), but instead of following the order and the points in the phase space according to the dynamics (3.3), we operate in a random fashion. More precisely, each element of a given matrix is chosen independently of all the others, and each matrix independently of the following one. This choice represents the simplest nontrivial approximation of the deterministic dynamics in the highly chaotic regime. It has already been shown in some cases that the scaling behavior of λ_i as a function of α does not change when the deterministic dynamics[5] is substituted by a random evolution.[6]

Since we are here interested in a comparison with the models studied in Sections 2 and 3, the only matrix elements kept different from zero are

those for which $|i-j|<1$, plus the pairs $(1, N)$, $(N, 1)$. Their probability distribution has been chosen according to the relation

$$a_{ij} = x_m^{\gamma}/2 + \bar{x}, \qquad m = 1, 2 \tag{4.3}$$

where $\bar{x}$ is a fixed value, γ is an odd integer, and x_m is a random number either with a uniform distribution in the interval $(-1, 1)$ $(m=1)$, or with a Gaussian distribution with zero average and unit variance $(m=2)$.

Moreover, one can impose the analogy of the conservation of total momentum $\sum_{i=1}^{N} p_i(n) = 0$ by requiring

$$\sum_{j=1}^{N} a_{ij} = 0, \qquad \forall i \tag{4.4}$$

We have verified that the results for the LCE do not vary significantly for different choices of the probability distribution. In Fig. 6 we show a typical LCE spectrum reproducing the same qualitative features observed for all models studied in Sections 2 and 3 (for other cases, see Ref. 6). In contrast to the models of the previous sections, here the shape of the LCE spectrum is fairly independent of α. However, since the enhancement (for small α) of the LCE spectrum around λ_1 is related to the long-time correlations in the deterministic dynamics, we could not expect an agreement in that parameter region.

Another recipe to construct these random matrices is obtained by keeping the formal definition of the matrix elements as in Eq. (4.2), but

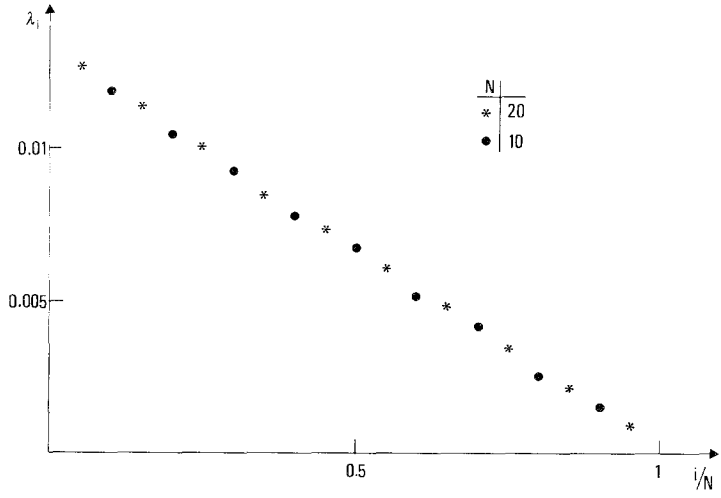

Fig. 6. Liapunov exponents λ_i versus i/N, for random matrices (4.3), $\gamma=3$, $\alpha=0.01$, $\bar{x}=0$.

choosing the phase point $\mathbf{q}(n)$ in a random fashion. Moreover, in order to have a strict analogy with the dynamics of the symplectic map (3.3), we have chosen the coordinates q_i to be identically and uniformly distributed in the interval $(0, 2\pi)$. Indeed, several simulations have confirmed this to be the asymptotic distribution. Therefore, our procedure consists, first, in choosing a random sequence of points in the phase space and, second, in multiplying the matrices associated to the tangent space. Apart from the correlations present in the deterministic evolution, the main difference between the two procedures comes from the existence of stable and unstable manifolds in the map (3.3). In particular, from the alignment of the Liapunov vector along the unstable manifold, it follows that the closer

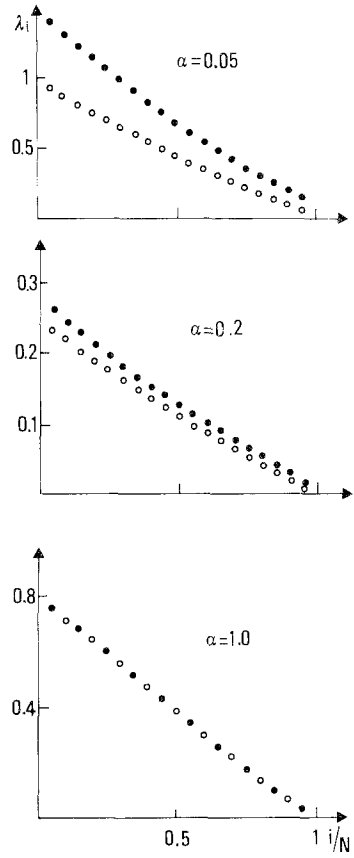

Fig. 7. Liapunov spectrum of (●) model (3.3) with $g(x) = \sin x$ and (○) random matrices (4.5), at different α.

a point is to its nth iterate, the closer are the directions of the Liapunov vectors of the respective points. The same cannot obviously be expected for random matrices, because of the random ordering. However, in spite of this difference, the numerical results for the two models do coincide for large α's, as shown in Fig. 7 [for $g(x) = \sin x$], where the respective LCE spectra are reported. We have not been able to find a reasonable conjecture substantiating this numerical result. Its importance is, however, transparent, as it allows one to quantify the effect of the correlations in the deterministic flow: the difference between the LCE spectrum for the symplectic maps and random matrices is entirely due to the correlations.

5. CONCLUSIONS

The wide phenomenology presented here of symplectic dynamics shows that the existence of a thermodynamic limit for the LCE spectrum is a generic result. Moreover, the shape of this spectrum in the strongly chaotic limit is almost independent of the details of the dynamics and is approximatively linear. Similar results have been obtained by analytic computations for some stochastic linear dynamical systems, thus suggesting a sort of universality in the high-dimensional limit.[7] This is a first encouraging result toward the construction of a statistical approach to high-dimensional symplectic models. Another relevant result is the squeezing of the LCE spectrum near $x = 0$ as an integrable limit is approached. This suggests that a few variables contribute to a chaotic motion on a short time scale, while all the others perhaps yield, a very slow diffusion. In other words, the fast chaotic behavior is confined to a low-dimensional manifold. This is analogous to what happens in some dissipative systems, where the center manifold theory[8] allows, in principle, the identification of the subspace of the chaotic motion, with the obvious difference that the other variables do not contribute at all to the asymptotic motion.

APPENDIX

Here we report a brief sketch of the numerical algorithm for computing the LCE spectrum. Let us consider the equation of motion

$$\dot{\mathbf{x}} = \mathbf{f}(\mathbf{x}), \qquad \mathbf{x}(t+1) = \mathbf{g}(\mathbf{x}(t)) \tag{A.1}$$

where $\mathbf{x}$, $\mathbf{f}$, $\mathbf{g} \in R^{2N}$. The evolution in the tangent space is described by

$$\dot{J}_i = \sum_{m=1}^{2N} \frac{\partial f_i}{\partial x_m} J_m, \qquad J_i(t+1) = \sum_{m=1}^{2N} \frac{\partial g_i}{\partial x_m} J_m(t) \tag{A.2}$$

where the derivatives are evaluated along the trajectory $\mathbf{x}(t)$ determined by Eq. (A.1). The Liapunov exponents are finally given by[9]

$$\sum_{i=1}^{l} \lambda_i = \lim_{t \to \infty} \frac{1}{t} \ln |\mathbf{J}^{(1)}(t) \times \cdots \times \mathbf{J}^{(l)}(t)| \tag{A.3}$$

where $J^{(m)}(t)$ evolves according to Eq. (A.2), and $J^{(m)}(0)$ are orthonormal vectors with unitary norm. In practice, Eq. (A.3) cannot be used directly to compute the LCE, since the angles among the $J^{(m)}(t)$ tend to zero for t tending to infinity. A repeated application of the Gram–Schmidt orthonormalization procedure, however, allows one to overcome the difficulty. For more details see Ref. 9.

REFERENCES

1. J. P. Eckmann and D. Ruelle, *Rev. Mod. Phys.* **57**:617 (1985).
2. R. Livi, M. Pettini, S. Ruffo, M. Sparpaglione, and A. Vulpiani, *Phys. Rev. A* **31**:1039 (1985); R. Livi, M. Pettini, S. Ruffo, and A. Vulpiani, *Phys. Rev. A* **31**:2740 (1985).
3. Ya. B. Pesin, *Dokl. Akad. Nauk* **226**:774 (1976).
4. R. Livi, A. Politi, and S. Ruffo, *J. Phys. A* **19**:2033 (1986).
5. A. B. Rechester, N. M. Rosenblut, and R. B. White, *Phys. Rev. Lett.* **42**:1247 (1979); G. Benettin, *Physica* **13D**:211 (1984).
6. G. Paladin and A. Vulpiani, *J. Phys. A* **19**:1881 (1986); G. Parisi and A. Vulpiani, *J. Phys. A* **19**:L425 (1986); B. Derrida and E. Gardner, *J. Phys. (Paris)* **45**:1283 (1984).
7. C. M. Newman, *Commun. Math. Phys.* **103**:121 (1986); "Liapunov exponents for some products of random matrices: Exact expressions and asymptotic distributions," to appear in *Random Matrices and Their Applications*, J. E. Cohen, M. Kesten and C. M. Newman (eds.), AMS Series in Contemporary Mathematics.
8. J. Carr, *Applications of Centre Manifold Theory* (Springer, New York, 1981).
9. G. Benettin, L. Galgani, A. Giorgilli, and J. M. Strelcyn, *Meccanica* **15**:9, 15 (1980).